Liquid Crystals
Publication details, including instructions for authors and subscription information:
http://www.informaworld.com/smpp/title~content=t713926090

Molecular dynamics and conformational behaviour of mesogenic resorcinarenes

Enrico Dalcanale[a]; Giancarlo Antonioli[b]; Mauro Ricco[b]; Herbert Groothues[c]; Friedrich Kremer[c]
[a] Dipartimento di Chimica Organica e Industriale, Universita di Parma, Parco Area delle Scienze 17/A, I-43100 Parma, Italy, [b] Dipartimento di Fisica e INFM, Universita di Parma, Parco Area delle Scienze 7/A, I-43100 Parma, Italy, [c] Fakultat Physik und Geowissenschaften, Universitat Leipzig, Linnestrasse 5, D-04103 Leipzig, Germany,

Online publication date: 06 August 2010

To cite this Article Dalcanale, Enrico , Antonioli, Giancarlo , Ricco, Mauro , Groothues, Herbert and Kremer, Friedrich(2000) 'Molecular dynamics and conformational behaviour of mesogenic resorcinarenes', Liquid Crystals, 27: 9, 1161 — 1169
To link to this Article: DOI: 10.1080/02678290050122006
URL: http://dx.doi.org/10.1080/02678290050122006

LIQUID CRYSTALS, 2000, VOL. 27, NO. 9, 1161–1169

Molecular dynamics and conformational behaviour of mesogenic resorcinarenes

ENRICO DALCANALE*
Dipartimento di Chimica Organica e Industriale, Università di Parma,
Parco Area delle Scienze 17/A, I-43100 Parma, Italy

GIANCARLO ANTONIOLI, MAURO RICCÒ
Dipartimento di Fisica e INFM, Università di Parma,
Parco Area delle Scienze 7/A, I-43100 Parma, Italy

HERBERT GROOTHUES and FRIEDRICH KREMER
Fakultät Physik und Geowissenschaften, Universität Leipzig, Linnéstrasse 5,
D-04103 Leipzig, Germany

(*Received 20 December 1999; accepted 26 February 2000*)

The dynamic and conformational behaviour of four mesogenic resorcinarenes exhibiting columnar mesophases have been studied by a combination of broadband dielectric spectroscopy and deuterium solid state NMR. Broadband dielectric spectroscopy provided evidence for two relaxation processes present both in the mesophase and in the isotropic liquid. The high frequency process II, common to all mesogens, has been assigned to the libration of the carbonyl groups of the ester junctions between the core and the side chains. The low frequency process I, present in conformationally mobile mesogens **1** and **2**, has been attributed to the ring inversion process of the macrocyclic core associated with dipole inversion along the columnar axis. Deuterium solid state NMR performed on **4**, the deuteriated analogue of **1**, confirmed the molecular dynamics attribution for process I, assigning the ring inversion to the interconversion of the two equivalent crown conformations.

1. Introduction

Polar achiral liquid crystals have attracted considerable attention in recent years, both from the theoretical and the applicative points of view [1–3]. Among them, bowlic mesogens are an interesting class of liquid crystalline materials, since the asymmetric three dimensional shape of their macrocyclic cores can lead to the formation of polar columnar phases with potential ferroelectric properties [4, 5]. The switching of the dipolar electric moments along the molecular symmetry axis, associated with the conformational ring inversion process of the macrocyclic cores, constitutes a further interesting feature [6, 7]. In this respect the understanding of molecular dynamics and conformational behaviour of bowlic mesogens in the mesophase is determinant for the design of new liquid crystalline bistable systems based upon them. Here we report the results of a study on the molecular dynamics in mesogenic resorcinarenes using the combination of dielectric spectroscopy and deuterium solid state NMR spectroscopy.

Dodecasubstituted resorcinarenes **1–3** (figure 1) display columnar mesophases, where the macrocycles are stacked to form columns, while the surrounding alkanoyloxy side chains are liquid-like [8]. The conformational mobility of the macrocyclic cores depends on the nature of the substitution at the bridging carbon atoms: for hydrogen (compounds **1** and **2**) the ring inversion process is observed in solution [9] and therefore possible in the isotropic and columnar phases, while for CH_3 (compound **3**) it is inhibited, as proved by deuterium solid state NMR studies performed on selected deuteriated derivatives [10]. Since the ring inversion process leads to an inversion of the electric dipole moment of the molecules within the columns, dielectric spectroscopy is an ideal method for comparing the molecular dynamics of different macrocycles, while deuterium NMR is a powerful technique for studying their conformational behaviour in the mesophase [11, 12].

*Author for correspondence; e-mail: dalcanal@unipr.it

Liquid Crystals ISSN 0267-8292 print/ISSN 1366-5855 online © 2000 Taylor & Francis Ltd
http://www.tandf.co.uk/journals

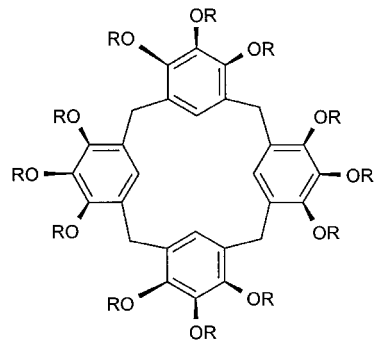

1-2

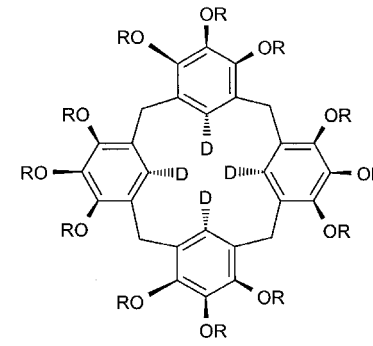

4

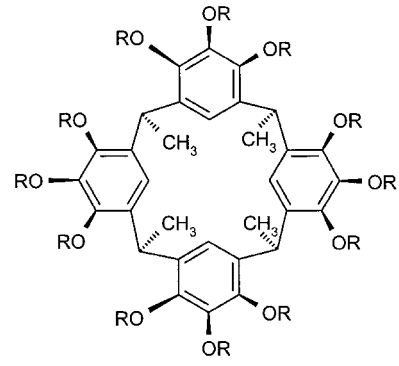

3

Figure 1. Molecular structures of the four compounds investigated: **1** $R = CO–C_9H_{19}$; **2** $R = CO–C_{11}H_{23}$; **3** $R = CO–C_{15}H_{31}$; **4** $R = CO–C_9H_{19}$.

2. Experimental

2.1. *Synthesis*

ACS grade reagents were used without further purification. Flash chromatography was performed using silica gel 60 (Merck, 230–400 mesh ASTM). Analytical TLC was carried out on precoated silica gel 60 plates. NMR spectra in solution were recorded on a Bruker AMX 400 spectrometer. Mass spectra were recorded on a Finnigan MAT SSQ 710 using the CI technique. Transition temperatures were measured using a Perkin-Elmer DSC 7 thermal analyser. Optical textures were observed with a Leitz-Panphot polarizing microscope, equipped with a Mettler FP 82 hot stage.

Compounds **1–3** were prepared according to published procedures [9, 13].

Compound **4**, 25,26,27,28-tetradeuterio-pentacyclo-[19.3.1.1^{3,7}.1^{9,13}.1^{15,19}]octacosa-1(25),3,5,7(28),9,11,13(27),15,17,19(26),21,23-dodecaene 4,5,6,10,11,12,16,17,18,22,23,24-dodecadecanoate, was prepared as follows. To a solution of 1.59 g (12 mmol) of 1,2,3-pyrogallol-d_6 (synthesized following the procedure for the preparation of 1,4-hydroquinone-d_6) [14]) in 20 ml of water and 4 ml of hydrochloric acid 37%, 620 µl (9 mmol) of 40% formaldehyde were added at room temperature under argon. After 2 h the pale pink precipitate formed was collected by filtration, washed with water to neutrality and dried under vaccum to give 457 mg of deuteriated macrocyclic precursor (28% yield). To this solid 7 ml (34 mmol) of decanoyl chloride were added and the resulting mixture was stirred at 120°C for 2 h. The excess of acyl chloride was removed by vacuum distillation (5×10^{-2} mm Hg/37°C) to give a waxy solid which was dissolved in dichloromethane. The organic phase was shaken with 0.2 M sodium hydroxide, washed with water to neutrality and dried over sodium sulphate. After filtration and evaporation of the solvent, the residue was purified by flash chromatography with hexane/ethyl acetate 9/1 as eluant to give 1.18 g of **4** as a white solid (60% yield).

^{1}H NMR ($CDCl_3$): δ 0.89 (t, 36H, CH_3); 1.24 (bs, 144H, CH_2 chains); 1.60 (m, 24H, CO–CH_2–CH_2); 2.40 (m, 24H, CO–CH_2); 3.61 (s, 8H, CH_2 macrocycle);

6.53 (s, residual Ar–H). ^{1}H NMR analysis indicated a deuteriation grade > 90%. ^{2}H NMR ($CHCl_3$): δ 6.5 (bs, Ar–D). MS(CI): m/z cluster centred at $MH^+ = 2409$ (100%).

2.2. *Mesomorphic properties*

The transition temperatures of mesogens **1–4** are given in the table at DSC heating–cooling rates of 10°C min^{-1}. Wider mesophase temperature ranges were obtained if slower heating–cooling rates were applied. In the case of **3**, for instance, at a cooling rate of 1°C min^{-1} the mesophase temperature range becomes 284°C < Col_{ho} < 336°C. Miscibility studies between **4** and its non-deuteriated derivative **1**, whose mesophase has already been characterized as Col_r [9], confirmed the structural attribution for **4**.

2.3. *Broadband dielectric spectroscopy measurements*

The dielectric measurements up to 10^7 Hz were carried out with a frequency response analyser (Schlumberger SI 1260). At low frequencies the impedance of the sample circuit exceeds $10^8\ \Omega$ which is above the limit of the SI 1260. To overcome this limitation we used an active sample cell (Novocontrol BDC) which performs a current to voltage conversion of the sample signal and amplifies the signal to 10–30 mV. By this method impedance measurements up to $10^{14}\ \Omega$ are possible. The sample capacitor consists of two gold covered brass electrodes 20 mm in diameter separated by 50 µm. In order to get a good electric contact, the capacitor was filled with the dielectric material at temperatures above the clearing point. With this set-up, the resolution in tan δ is better than 10^{-3} in the frequency range from 10^{-3} Hz to 5×10^6 Hz. Temperature is controlled by a gas heating system based on evaporation of liquid nitrogen (Novocontrol Quatro). The temperature can be varied in the range from − 160°C up to 400°C with a precision of 0.01°C.

Table. Transition temperatures (°C) for **1–4**.[a]

Compound	Transition[b]	T/°C	Transition[c]	T/°C
1	I–Col_r	338	Cr–Col_r	339.5
	Col_r–Cr	306	Col_rI	353.5
2	I–Col_r	327	Cr–I[d]	347
	Col_r–Cr	311		
3	I–Col_{ho}	328.5	Cr–Col_{ho}	321
	Col_{ho}–Cr	300	Col_{ho}–I	334
4	I–Col_r	338	Cr–Col_r	338
	Col_r–Cr	308	Col_r–I	353

[a] These results refer to DSC measurements, 10°C min^{-1}. Cr = crystal form; Col_r, Col_{ho} = columnar rectangular and columnar hexagonal ordered mesophases, respectively; I = isotropic liquid.
[b] Cooling run.
[c] Second heating run.
[d] Mesophase is monotropic.

2.4. *Deuterium solid state NMR measurements*

The spectra in condensed phases were recorded using a Stelar Spinmaster 300 MHz spectrometer. All the samples had been degassed and sealed under vacuum in Pyrex ampules. Spectra were recorded using a quadrupolar spin-echo sequence ($t_{\pi/2} = 5$ µs) with a minimum pulse separation in order to avoid distortion of spectra due to acoustic ringing effects ($\tau = 25$ µs). Good quality spectra were observed only when the mesophase was reached by slowly (4°C h^{-1}) cooling the sample from the isotropic phase ($T > 353$ K). This procedure partially aligns the columnar axes in the mesophase along the external magnetic field; this was confirmed by the analysis of the spectra. The quadrupolar interaction parameters of the aromatic deuterons, $\nu_Q = 120$ kHz and $\eta = 0.07$ have been determined from a low temperature experiment ($T \sim 77$ K).

3. Broadband dielectric spectroscopy

For a quantitative analysis the dielectric data were fitted with a generalized relaxation function according to Havriliak and Negami [15]:

$$\varepsilon^* = \varepsilon' - i\varepsilon'' = \varepsilon_\infty + \frac{\varepsilon_S - \varepsilon_\infty}{[1 + (i\omega\tau_{HN})^\alpha]^\gamma} \qquad (1)$$

In this notation ε_∞ stands for the dielectric permittivity of induced polarization and ε_S for the dielectric permittivity in the case of a static field; ω is the angular frequency of the applied electric field. The dielectric strength $\Delta\varepsilon$ is defined by $\Delta\varepsilon = \varepsilon_S - \varepsilon_\infty$, and α and $(-)\alpha\gamma$ characterize the logarithmic slope of the low-frequency and high frequency side of the single relaxation process, respectively. The conductivity contribution was taken into account by equation (2)

$$\varepsilon''(\omega) = \frac{\sigma_0 a}{\omega^s \varepsilon_0} \qquad (2)$$

where σ_0 is the direct current conductivity and ε_0 the permittivity of free space. For Ohmic behaviour $s = 1$; deviations ($s < 1$) are caused by electrode polarization. a is a factor having the dimensions $[a] = (\text{Hz})^{1-s}$ for $s \neq 1$.

The molecular structures of compounds **1–4** are shown in figure 1 and their phase transitions are reported in the table. Mesogens **1** and **2** present the same macrocyclic core with side chains of different length. This structural difference alters the phase behaviour: **1** forms an enantiotropic columnar mesophase (Col_r), while the Col_r phase of **2** is monotropic and restricted to a narrower temperature range.

Figure 2 compares the dielectric loss (ε'') of both compounds **1** and **2** in the crystalline (*a*), liquid crystalline (*b*) and isotropic phases (*c*). The increase of ε'' at the low frequency side, which is observed in each phase, originates from a charge transport mechanism of ionic impurities. In the crystalline phase for both compounds, one relaxation process can be detected. It has a broad relaxation time distribution and its dielectric strength is weak, compared with the high temperature phases ($\varepsilon''_{max} \approx 10^{-2}$). In the columnar mesophase, figure 2 (*b*), two well separated dispersion regions can be detected for both compounds. The low and high frequency processes will be further referred to as process I and II, respectively, as evidenced in figure 3 in the case of **1**. Due to the monotropic mesophase behaviour of **2**, the thermal history has a distinct influence on the dielectric function. When the dielectric loss is measured in the heating run where no mesophase is formed, process I is suppressed, figure 2 (*b*). The dielectric loss in the isotropic phase is shown in figure 2 (*c*). The high frequency dispersion region seems to be identical for the two compounds. A closer look reveals an asymmetric loss peak for both of them. While for compound **1** it is not possible to make a reliable separation of the dispersion region into two Havriliak–Negami functions, for compound **2** an accurate analysis of ε'' reveals two overlapping relaxations.

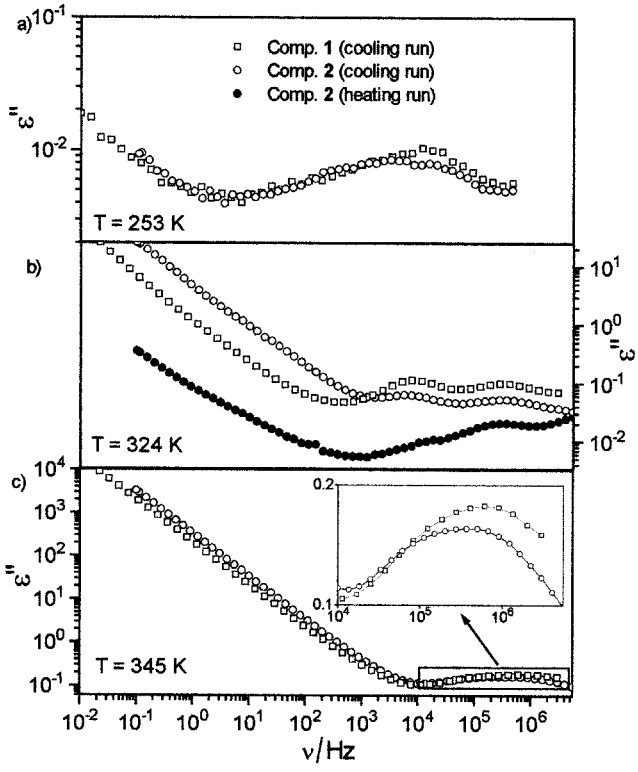

Figure 2. Dielectric loss (ε'') versus frequency for compounds **1** and **2** in the (*a*) crystalline phase, (*b*) columnar mesophase and (*c*) isotropic phase. Except for the filled circles in (*b*) all measurements were started in the isotropic phase and then made successively as the sample was cooled to lower temperatures. The filled circles in (*b*) show the dielectric loss of compound **2** in the crystalline phase because of the monotropic mesophase behaviour. The inserted plot in (*c*) is a magnification of the plot area represented by the rectangle.

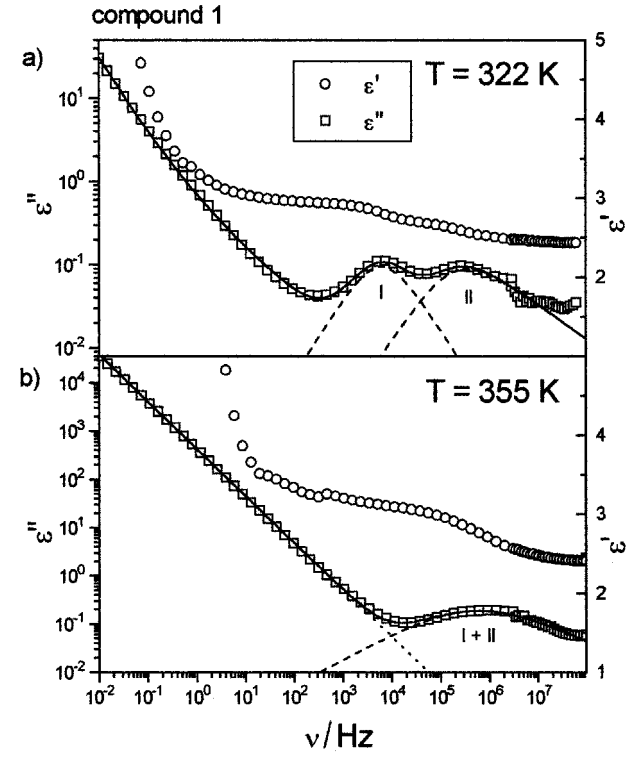

Figure 3. Real (ε') and imaginary part (ε'') of the dielectric function versus frequency for compound **1**: (*a*) in the columnar mesophase (T = 322 K) and (*b*) in the isotropic phase (T = 355 K). The dashed lines represent the contributions of the single relaxation processes to ε''. The solid line is the sum of the relaxation and conductivity contributions. Havriliak–Negami fit-parameter. Process I (T = 322 K): $\Delta\varepsilon = 0.217$, $\alpha = 0.92$, $\gamma = 1$, $\tau_{max} = 3 \times 10^{-5}$ s; process II (T = 322 K): $\Delta\varepsilon = 0.31$, $\alpha = 0.86$, $\gamma = 0.49$, $\tau_{max} = 9.2 \times 10^{-7}$ s.

Both the real and imaginary part of the dielectric function are shown for **1** in figure 3. The contributions of the single relaxations to ε'' are indicated by dashed lines. In the isotropic phase the two relaxation processes have similar relaxation times and only one broad dispersion region is observed.

The temperature dependence of the mean relaxation times is shown in an activation plot (figure 4). The vertical lines in figure 4 indicate the temperature regions of the columnar mesophase for each compound. The activation diagram reveals that the one relaxation

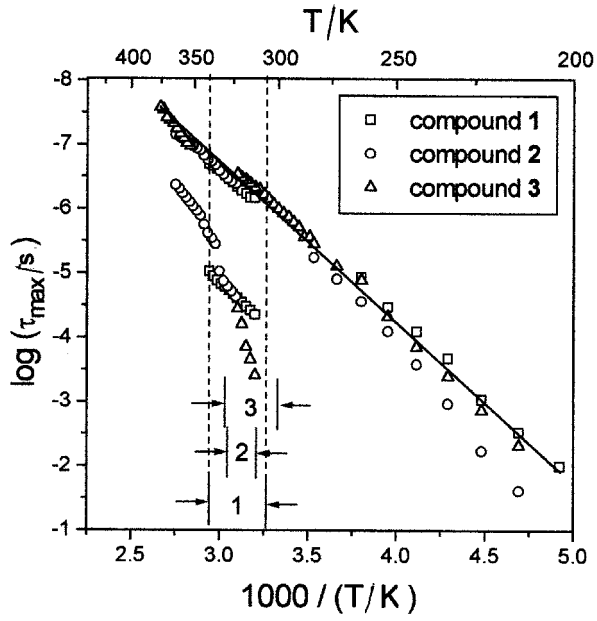

Figure 4. Arrhenius diagram for the mean relaxation times of the three mesogens. The vertical lines indicate the temperature ranges of the columnar mesophases determined from DSC cooling runs.

observed in the crystalline phase corresponds to the high frequency process II in the isotropic liquid and in the mesophase. It is Arrhenius-activated in the whole temperature range in the case of compound **1** ($\Delta E = 22.6 \pm 0.8\,\mathrm{kJ\,mol^{-1}}$). For macrocycle **2** it deviates from an Arrhenius behaviour at temperatures below 250 K. In **2** the mean relaxation times of the two processes are split by a factor of approximately ten in the isotropic phase, which is at the limit that can be unambiguously separated. For compound **1** no clear separation into two relaxations is possible in the isotropic phase. Cooling into the columnar mesophase leads to a strong shift of the low frequency process towards longer relaxation times in both compounds (figure 4). Since process II is not influenced by the phase transitions, its molecular assignment must be a localized motion. We assign it to a libration involving the carbonyl units in the side chains; this is commonly named the β-relaxation (in compounds containing similar ester structures, dielectric relaxations with identical activation energies have been observed) [16]. The low frequency process I observed by dielectric spectroscopy exists only in the isotropic and columnar phases. The influence of the phase on the dynamics shows up when the dielectric loss values of the monotropic columnar mesophase and the crystalline phase of compound **2** are compared at the same temperature, figure 2 (*b*). While the β-relaxation is just decreased in its dielectric strength in the crystalline phase, the low frequency process has nearly disappeared. Supported by the NMR results (see next section) we assign process I to the ring inversion of the macrocyclic core. In the mesophase, the ring inversion is sterically hindered by the columnar packing leading to longer mean relaxation times compared with the isotropic phase. The same effect has been observed in macrocyclic oligoethyleneamine derivatives [17]. Compound **3** is stereoselectively substituted with four methyl groups at the ring methylene units. This substitution completely suppresses the ring inversion process [18]. Figure 5 shows the dielectric loss of this compound in the columnar mesophase. In addition to the high frequency β-relaxation and the conductivity contribution, a low frequency process can be detected for **3**, with a similar mean relaxation time, but much weaker dielectric strength compared with process I of **1** and **2**. Hence, despite the restriction of the conformational mobility of the macrocyclic core, small angle fluctuations of the ring system exist in the columnar mesophase of **3**.

4. Deuterium solid state NMR spectroscopy

Deuterium solid state NMR spectroscopy was applied for studying the conformational behaviour in the mesophase of the macrocycle of compound **4**, the deuteriated

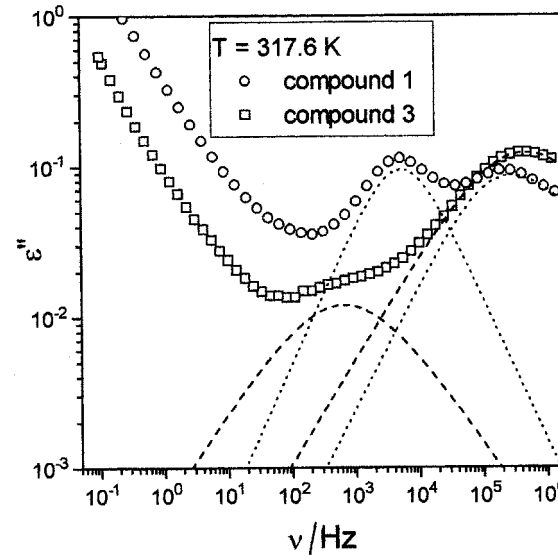

Figure 5. Dielectric loss versus frequency for compounds **1** and **3** in the columnar mesophase. The dotted and dashed lines represent the contributions of the single relaxations to the dielectric loss of **1** and **3**, respectively. Havriliak–Negami fit-parameter—Compound **1** ring inversion process: $\Delta\varepsilon = 0.21$, $\alpha = 0.94$, $\gamma = 1$, $\tau_{HN} = 3.3 \times 10^{-5}$ s; β-process: $\Delta\varepsilon = 0.3$, $\alpha = 0.83$, $\gamma = 0.53$, $\tau_{HN} = 1.1 \times 10^{-6}$ s. Compound **3** ring inversion process: $\Delta\varepsilon = 0.043$, $\alpha = 0.65$, $\gamma = 0.98$, $\tau_{HN} = 2.5 \times 10^{-4}$ s; β-process: $\Delta\varepsilon = 0.45$, $\alpha = 0.70$, $\gamma = 0.74$, $\tau_{HN} = 5 \times 10^{-7}$ s.

analogue of **1**. The core of the molecule was selectively deuteriated in the aromatic positions, which are diagnostic of the possible inversion dynamics of the macrocyclic core through a $\sim 70°$ jump in the C–D bond orientation. The spectrum observed in the mesophase has been simulated assuming a stochastic markovian two-site exchange stationary process. Further corrections of the simulated spectrum were introduced taking into account the partial alignment of the sample in the mesophase induced by the applied magnetic field and the possible line shape distortion due to the quadrupolar spin-echo sequence.

4.1. *Theory*

We briefly outline the theory adopted in our line shape simulation based on the two-site exchange model [19]. The general form of the spin hamiltonian H_T is expressed as the scalar product of spherical tensorial operators of rank two:

$$H_T = \sum_{k=0}^{2} \sum_{q=-k}^{k} (-1)^q A_{kq} T_{k-q} \tag{3}$$

where A_{kq} depends on spin coordinates, while T_{k-q} depends on spatial (angular in our case) coordinates α, β, γ representing the orientation of the tensor interaction in the laboratory reference frame. According to our dynamic model, the angles $\alpha(t)$, $\beta(t)$, $\gamma(t)$ are considered as stochastic variables and represent the time dependence of H_T. The tensor interaction in our case is the quadrupolar interaction of ^{2}H nuclei with the electric field gradient originating from the C–H bond (it is reasonable to assume that one of the tensor principal axes is collinear with the bond direction). Following a perturbative approach ($\omega_Z \gg \omega_Q$) its two eigen frequencies for a spin $S = 1$ are:

$$\omega_+ = \omega_0 + \left(\frac{8}{3}\right)^{1/2} T_{20} \tag{4}$$

where $\omega_0 = \gamma_D H$

$$\omega_- = \omega_0 - \left(\frac{8}{3}\right)^{1/2} T_{20}. \tag{5}$$

In order to compute the angular dependence of these two frequencies [i.e. $T_{20}(\alpha(t), \beta(t), \gamma(t))$] different rotations connecting the principal axis system (P) to the molecular system (M) and finally the laboratory system (L) have to be taken into account:

$$(X_P, Y_P, Z_P) \xrightarrow{R'(\alpha,\beta,\gamma)} (X_M, Y_M, Z_M) \xrightarrow{R(\varphi,\vartheta,\psi)} (X_L, Y_L, Z_L \| \mathbf{H})$$

defining the total rotation operator: $R_{tot} = R'(\alpha, \beta, \gamma) R(\varphi, \vartheta, \psi)$ we get for T_{20}:

$$\begin{aligned} T_{20}^{(L)}(\alpha, \beta, \gamma) &= R_{total} T_{20}^{(P)} R_{total}^{-1} \\ &= \sum_{k,n} T_{2k}^{(P)} D_{kn}^{(2)}(\alpha, \beta, \gamma) D_{n0}^{(2)}(\varphi, \vartheta, \psi) \\ &= \sum_{k=-2}^{2} \sum_{n=-2}^{2} T_{2k}^{(P)} \exp(-i\alpha k) d_{kn}^{2}(\beta) \\ &\quad \times \exp(-i\gamma m) d_{n0}^{2}(\vartheta) \exp(-in\varphi) \end{aligned} \tag{6}$$

where $D_{kn}^{(2)}(\alpha, \beta, \gamma)$ are Wigner matrices of rank 2 and $d_{kn}^{2}(\alpha)$ their reduced form. From expression (6), straightforward but lengthy calculations give the explicit angular dependence of ω_+ and ω_-.

The change in orientation of the C–D bond from the orientation (site) i to the orientation j implies a sudden change in these two frequencies (referred to as ω) from ω_i to ω_j. The stationary markovian exchange process is described by an N sites exchange matrix whose elements Π_{ij} are the transition probability between the two sites i and j and:

$$\sum_{i=1}^{N} \Pi_{ij}(\omega_i, \omega_j) = 0. \tag{7}$$

If we suppose that the only relaxation mechanism is this two-site exchange, the time evolution of the deuterium nuclear magnetization of the j site can be described by:

$$\frac{d}{dt} M_j(t) = i\omega_j M_j + \sum_k \Pi_{jk} M_k \qquad j = 1 \ldots N \tag{8}$$

which can be solved in matrix form [19].

The spectrum intensity $I(\omega)$ is obtained by Fourier transforming the free induction decay (FID)

$$G(t) = \sum_{j=1}^{n} M_j(t). \tag{9}$$

In the case of the two-site exchange, the spectrum intensity can be expressed as:

$$I(\omega) = \frac{1}{2} \frac{k(\omega_1 - \omega_2)^2}{[(\omega - \omega_1)(\omega - \omega_2)]^2 + k^2[2\omega - (\omega_1 + \omega_2)]^2} \tag{10}$$

where $k = 1/\tau_c$ is the exchange frequency. The powder spectrum can be then calculated by performing the angular average based on the appropriate orientational distribution $f(\Omega)$ of the molecular macrocycle in the mesophase:

$$F(\omega) = \int_{\Omega} f(\Omega) I(\omega, \Omega) \, d\Omega. \tag{11}$$

4.2. *Results*

The ^{2}H NMR spectrum of **4** in the aligned mesophase at $T = 341$ K is shown in figure 6. Reasonable agreement between the simulated spectra shown below and that observed is obtained only in the case in which the crown conformation [9, 18] of the macrocycle is assumed.

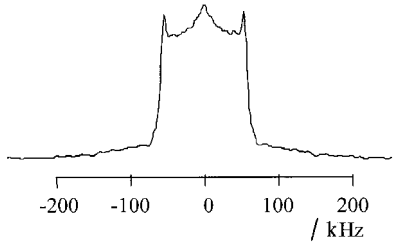

Figure 6. ^{2}H NMR spectrum of **4** in the aligned mesophase at $T = 341$ K.

The pair of frequencies ω_1 and ω_2 corresponding to a particular orientation (φ, ϑ) of the external magnetic field **H** in the molecular (M) reference frame are determined once the possible orientations of the tensor principal axes in the same reference frame are known. For our case we get:

$$(\alpha_1 = 0°, \beta_1 = 35, 1°, \gamma_1 = 0°)$$

and

$$(\alpha_2 = 0°, \beta_2 = \pi - \beta_1, \gamma_2 = 0°). \quad (12)$$

The value of β_1 is deduced from the structure of the crown conformation of the macrocycle. The field-induced alignment of the columnar axes requires the introduction of an order parameter $S = \langle P_2 \rangle$, which represents the second term of the expansion of the orientational

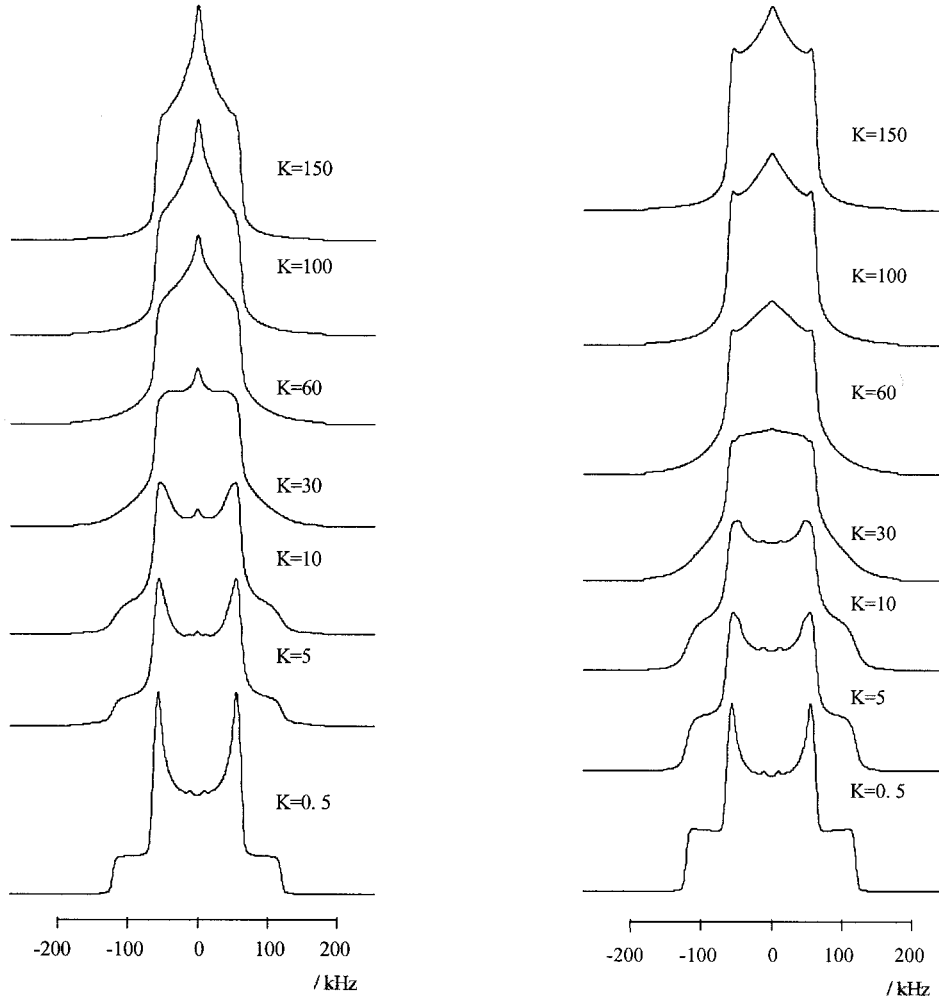

Figure 7. Simulation of ^{2}H NMR spectra for different jump-rate values K (kHz). The order parameter value is $S = 0.1$ ($\| \mathbf{H}$) left and $S = 0.34$ ($\| \mathbf{H}$) right.

distribution function into Legendre polynomials:

$$f(\vartheta) = \sum_{L} a_L P_L(\cos\vartheta) \tag{13}$$

$$a_N = (2N+1)\frac{\langle P_N \rangle}{2}. \tag{14}$$

Figure 7 displays the simulated spectra for different values of the jump-rate K for two different order parameter values: 0.1 and 0.34, respectively (the values used for $\nu_Q = 120$ kHz and $\eta = 0.07$ have been measured in an experiment at low temperature). In this case alignment has been supposed to take place along the field direction (longitudinal alignment). The simulated spectra in the case of alignment perpendicular to the magnetic field (transverse alignment) do not reproduce the observed line shape (figure 6). For the longitudinal alignment a better agreement is however obtained if the distortion effect originating from the pulse sequence is suitably taken into account, correcting the two-site exchange $I(\omega)$ as follows [20]:

$$J(\omega,\tau) = I(\omega)\left\{\begin{array}{c}\left(\cos\lambda\tau + \dfrac{k}{\lambda}\sin\lambda\tau\right)^2 + \dfrac{\Delta\omega^2}{\lambda^2}\sin^2\lambda\tau \\ (1+k\tau)^2 + \Delta\omega^2\tau^2 \\ \left(\cosh\rho\tau + \dfrac{k}{\rho}\sinh\rho\tau\right)^2 + \dfrac{\Delta\omega^2}{\rho^2}\sinh^2\rho\tau\end{array}\right\}$$
$$\begin{array}{ll} & (\lambda \equiv (\delta^2 - k^2)^{1/2},\ k^2 < \delta^2) \\ \times \exp(-2k\tau) & (k^2 = \delta^2) \\ & (\rho \equiv (k^2 - \delta^2)^{1/2},\ k^2 > \delta^2)\end{array} \tag{15}$$

where $\Delta\omega = \omega - \bar{\omega}$ and $\bar{\omega}$ is the average of the two frequencies ω_1, ω_2 while $\delta = (\omega_1 - \omega_2)/2$; $j(\omega, \tau)$ can be numerically integrated, as was done before, to give the powder spectrum. Figure 8 reports the simulated spectra for a longitudinal alignment and a pulse separation of

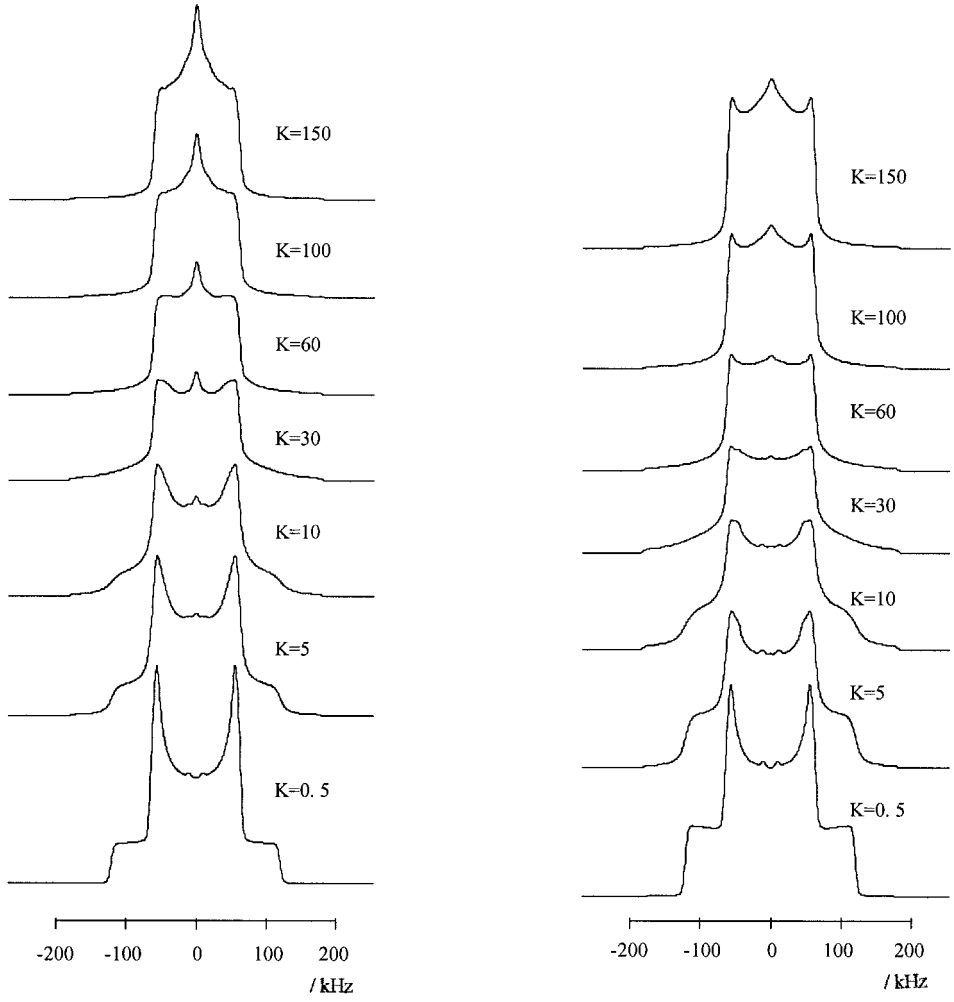

Figure 8. Simulation of ^{2}H NMR spectra for different jump-rate values K (kHz). Spectra corrected for pulse program distortion. The order parameter value is $S = 0.1$ ($\| \mathbf{H}$) left and $S = 0.34$ ($\| \mathbf{H}$) right.

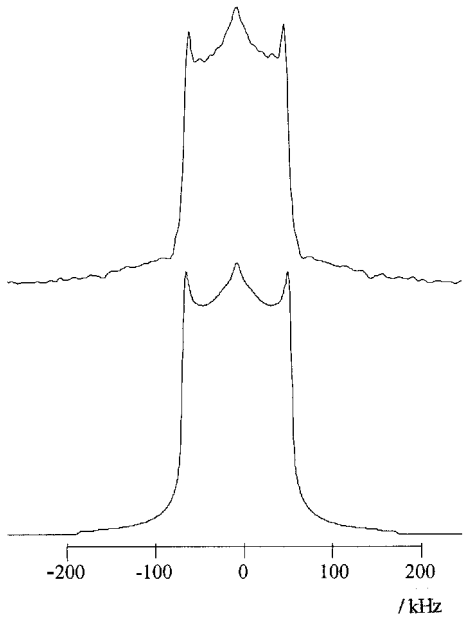

Figure 9. Comparison between the observed ^{2}H NMR spectrum (upper trace) and the simulation (lower trace) performed with the following parameters: $S = 0.34$ ($\| \mathbf{H}$), $K = 100\,\text{kHz}$, $\tau = 25\,\mu\text{s}$.

25 μs. The spectrum corresponding to $K = 100\,\text{kHz}$ and $S = 0.34$ reproduces quite well the line shape displayed in figure 6. Figure 9 displays a final comparison between the observed and simulated spectra. Definitely poorer agreement arises in the case of the transverse alignment.

The estimated rate for the ring inversion process $K = 100\,\text{kHz}$ in **4** nicely correlates with the low frequency process I observed in the dielectric relaxation experiments (figure 4) at the same temperature, supporting the molecular dynamics attribution.

5. Conclusions

Two relaxation processes were detected by broadband dielectric spectroscopy for mesogens **1** and **2** in their columnar and isotropic phases. The low frequency process I is ascribed to the inversion of the macrocyclic ring, while the high frequency process II is assigned to the libration of the carbonyl groups of the ester junctions between the core and the side chains (β-relaxation).

Deuterium solid state NMR measurements performed on the deuteriated derivative **4** showed the presence of a ring inversion process between two equivalent crown conformations in the columnar mesophase at a jump-rate $K = 100\,\text{kHz}$. This dynamics is associated with the dipole inversion along the molecular C_4 symmetry axis and hence must contribute to the dielectric function. The good agreement between the dielectric and NMR data in the temperature and frequency position of process I in the mesophase proves this molecular assignment. Moreover the complete suppression of the low frequency relaxation in the solid state clearly establishes that the activation of the ring inversion process is controlled by mesophase formation.

We acknowledge the Centro Interfacoltà di Misure of the University of Parma for instrumental facilities. This work was supported by MURST and INFM.

References

[1] Blinov, L. M., 1998, *Liq. Cryst.*, **24,** 143.
[2] Pelzl, G., Diele, S., and Weissflog, W., 1999, *Adv. Mater.*, **11,** 707.
[3] Berardi, R., Orlandi, S., and Zannoni, C., 1997, *J. chem. Soc., Faraday Trans.*, **93,** 1493.
[4] Lam, L. (Lin Lei), 1994, in *Liquid Crystalline and Mesomorphic Polymers*, edited by V. P. Shibaev and L. Lam (Berlin: Springer-Verlag), pp. 324–353.
[5] Lin Lei, 1987, *Mol. Cryst. liq. Cryst.*, **146,** 41–54.
[6] Zimmermann, H., Poupko, R., Luz, Z., and Billard, J., 1985, *Z. Naturfors. (a)*, **40,** 149.
[7] Malthête, J., and Collet, A., 1987, *J. Am. chem. Soc.*, **109,** 7544.
[8] Dalcanale, E., 1996, in *Comprehensive Supramolecular Chemistry*, Vol. 10, edited by D. N. Reinhoudt (Oxford: Elsevier Science), pp. 585–635.
[9] Cometti, G., Dalcanale, E., du Vosel, A., and Levelut, A. M., 1992, *Liq. Cryst.*, **11,** 93.
[10] Riccò, M., and Dalcanale, E., 1994, *J. phys. Chem.*, **98,** 9002.
[11] Speilberg, N., Sarkar, M., Luz, Z., Poupko, R., Billard, J., and Zimmermann, H., 1993, *Liq. Cryst.*, **15,** 311.
[12] Kuebler, S. C., Boeffel, C., and Spiess, H. W., 1995, *Liq. Cryst.*, **18,** 309.
[13] Bonsignore, S., Cometti, G., Dalcanale, E., and du Vosel, A., 1990, *Liq. Cryst.*, **8,** 639.
[14] Zimmermann, H., 1989, *Liq. Cryst.*, **4,** 591.
[15] Havriliak, S., and Negami, S., 1966, *J. polym. Sci.*, **C14,** 99.
[16] Vallerien, S. U., Werth, M., and Kremer, F., 1990, *Liq. Cryst.*, **8,** 889.
[17] Groothues, H., Kremer, F., Plesnivy, T., and Ringsdorf, H., 1996, *Macromol. Chem. Phys.*, **197,** 3881.
[18] Abis, L., Dalcanale, E., du Vosel, A., and Spera, S., 1990, *J. chem. Soc., Perkin Trans. 2*, 2075.
[19] Mehring, M., 1983, *High Resolution NMR in Solids* (Berlin: Springer-Verlag).
[20] Spiess, H. W., and Sillescu, H., 1981, *J. magn. Res.*, **42,** 381.